Journal of Materials Chemistry A

Accepted Manuscript

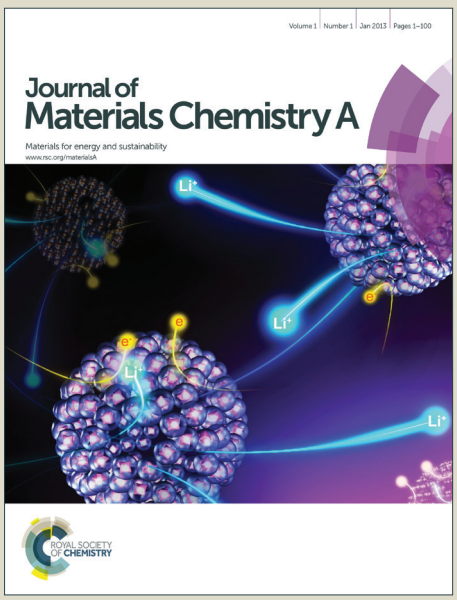

ROYAL SOCIETY OF CHEMISTRY

www.rsc.org/materialsA

Facile Fabrication of Multifunctional Perfluoroalkyl Functionalized Graphene Hydrogel via a Synchronous Reduction and Grafting Strategy

Ting Li, Yunqiao Ding, Libin Liu*, Jian Liu, Wenyuan Fang, Yu Xiang, Tianduo Li

Shandong Provincial Key Laboratory of Fine Chemicals, Key Laboratory of Fine Chemicals in Universities of Shandong, Qilu University of Technology, Jinan 250353, China

Corresponding authors: Fax: +86 531 89631208, E-mail: lbliu@qlu.edu.cn (L. B. Liu)

Abstract

Fluorine containing groups represent very promising functionalities due to that fluorine not only changing the physico-chemical properties of graphene surface, it may also alter its electronic and magnetic properties. Herein, we describe for the first time the synthesis and characterization of perfluoroalkyl functionalization of graphene oxide by a simple and general solution-based process via using perfluorooctyl functionalized aniline (R_F-NH_2) as reducing and grafting reagent synchronously. Importantly, the perfluoroalkyl functionalized graphene hydrogels (FGHs) could be achieved by a hydrothermal method. The as-fabricated FGHs exhibit outstanding absorption ability and electrochemical performances including ultrahigh specific capacitances of 321.6 F g^{-1} and excellent cycling stability in the aqueous electrolyte and organic electrolyte. The changes of electronic structure of the perfluoroalkyl functionalized graphene were also simulated by the density functional theory.

1. Introduction

Graphene, a typical two-dimensional planar monolayer of sp^2 carbon atoms, has attracted significant attention due to its outstanding electronic and mechanical properties.[1, 2] In order to realize the many potential applications that graphene can offer, the availability of graphene with a well defined and controllable surface and

interface properties is of critical importance. However, the strong π – π interaction between graphene sheets make them readily re-stack to form graphite-like powders or films, which limits their widely applications. Covalent functionalization techniques such as grafting of aryl group,[3] oxidation,[4] hydrogenation,[5, 6] and fluorination of graphitic material[7-9] are often adopted to modify graphene.

However, robust methods for producing covalent functionalization of pristine graphene possess considerable challenges due to its lack of reactive functional groups. The most common method for the covalent functionalization of graphene employs graphene oxide (GO) to prepare chemically modified graphene including GO and reduced GO (RGO).[10, 11] For example, Haddon and co-workers have functionalized GO with $SOCl_2$ and subsequent reaction with a long-chain aliphatic amine gave the amide derivative which is soluble in nonpolar solvents.[12] Another method employed by these authors is grafting aryl groups through diazotization reactions.[13] In addition, GO has been chemically modified by several other means with a porphyrin,[14] with an ionic liquid,[15] and with a terpyridine.[16] These new functionalities not only prevent restacking of graphene but also exhibit entirely different properties to those of graphene.

From this point of view, fluorine-containing groups represent very promising functionalities due to the high electronegativity and low free energy of fluorine. Introduction of fluorine into graphene not only can change the physico-chemical properties of graphene surface but also may alter its electronic and magnetic properties.[14, 17] Up to now, many fluorine-doped graphene has been synthesized by using XeF_2, plasma (CF_4 and SF_6) and HF as fluorinating agents, which effectively enlarge the application of graphene.[8, 18, 19] However, the use of these agents has some disadvantages. For example, XeF_2 requires high thermal treatment temperature (about 350℃) during the fluorination process, which may result in inevitable aggregation of graphene. Moreover, these agents are too expensive and very harmful, which will limit their large-scale applications. Therefore, the development of an easy, low-cost and efficient synthesis route is highly desirable. To the best of our knowledge, there have been no previous reports describing the perfluoroalkyl functionalized graphene.

Nowadays, many studies have showed that GO can form a 3D hydrogel structures by various interactions including hydrogen bonding, coordination, electrostatic interaction, and π-π stacking. Such graphene-based 3D hydrogels are conductive, mechanical stability and can be applied in many fields, such as energy storage and absorption.[20-26] However, perfluoroalkyl functionalized graphene hydrogels have not been reported so far.

Herein, we describe for the first time the synthesis and characterization of perfluoroalkyl functionalization of GO by a simple and general solution-based process via using perfluorooctyl functionalized aniline (R_F-NH_2) as reducing and grafting reagent synchronously (Figure 1a). Importantly, the perfluorootcyl functionalized hydrogel can also be achieved through hydrothermal method. As a proof-of-concept application, the hydrogels not only behave high absorption ability but also possess perfect electrochemical properties.

2. Materials and Methods

2.1 Materials

Natural graphite flakes (8000 mesh, purity 99.95%), Perfluorooctyl iodide, and 4-iodoaniline n-Octylamine were supplied by Aladdin, concentrated sulfuric acid (95–98%), concentrated hydrochloric acid (36–38%), Potassium permanganate, copper were all analytically pure and purchased from Beijing Chemical Factory (China). Hydrogen peroxide (H_2O_2) and sodium nitrate were supplied by LaiYang Shi Kant chemical company.

2.2 Syntheses of 4-(Perfluorooctyl) aniline (R_F-NH_2)

The dispersions of perfluorooctyl iodide (5.46 g, 0.01 mol), 4-iodoaniline (1.46 g, 0.0067 mol), and copper (1.28 g, 0.02 mol) in 25 ml DMSO were heated with stirring for 12 h at 120 ℃ in a three-necked 100 ml flask connected with a reflux condenser. The produced copper iodide and excess copper were removed by filtration. 10 ml water and 10 ml diethyl ether was added to the filtrate. The ether layer was washed several times with water to remove DMSO and perfluorooctyl iodide, and then purify

the product by column chromatography using hexane and diethyl ether (15:1) as eluent (1.2g, yield: 35.3%). ^{1}H-NMR (Chloroform-d) : 4.23 (br s, 2H), 7.54 (d, J= 8.8 Hz, 2H), 7.72 (d, J= 8.8 Hz, 2H).

2.3 Preparation of perfluoroalkyl functionalized graphene (FG)

Graphene oxide (GO) was prepared from natural graphite by the Hummers method (see supporting information). GO (0.6 g) was mixed with the solution of 4-(Perfluorooctyl) aniline (0.9 g) in 90 ml ethanol in a three-neck flask. The mixture was refluxed with stirring at 100 ℃ for 12 h or 24 h. Then the resulting solution was filtrated with a PP membrane with an average pore size of 0.22 μm. The filtrated powder was rinsed in 100 ml ethanol with the aid of ultrasonication for 5 min and then filtrated. The rinsing-filtration process was repeated for 4 times to remove the physically absorbed 4-(Perfluorooctyl) aniline. Finally, the mixture was dried in an oven at 80 ℃ for 24 h.

2.4 Fabrication of perfluoroalkyl functionalized graphene hydrogel (FGH)

The FGH can be easily prepared by heating a homogeneous mixture of GO (2 $mg \cdot mL^{-1}$ in H_2O) and 4-(Perfluorooctyl) aniline (1 $mg \cdot mL^{-1}$ in ethanol) without stirring at 100 ℃ for 12 h. Then the FGH was rinsed in water and repeated 5 times in order to remove the physically absorbed 4-(Perfluorooctyl) aniline. The FGHs with different mass ratios of 4-(Perfluorooctyl) aniline to GO (1:8, 1:4, 1:2) are marked as FGH-8, FGH-4, FGH-2, respectively.

2.5 Measurement of surface areas

MB dye adsorption method was employed to measure the specific surface areas of FGH. MB adsorption is a standard method for measuring the specific surface area of graphitic materials with 1 mg of adsorbed MB molecules covering 2.54 m^2 of surface area.[27] The surface areas were calculated by adding FGH into a standard concentration of MB in DI water for a total of 30 h to reach adsorption equilibrium. The MB concentration was determined by analyzing the supernatant through UV–Vis

spectroscopy at a wavelength of 665 nm and compared with the initial standard concentration of MB before interacting with FGH.

2.6 Adsorption Experiments

The adsorption experiments were carried out at room temperature to investigate the adsorption behaviors of MB onto the FGH-2. Typically, FGH-2 was placed into 100 mL MB aqueous solutions with different concentrations in a flask which was shaken in a rotary shaker for 30 h to reach adsorption equilibrium. After adsorption, the FGH-2 was directly removed from the solution, while the concentration of MB was determined by UV−vis absorption spectra. The adsorption capacities of the adsorbents were calculated according to the equation of $Q_e=(C_0-C_e)V/m$, where C_0 and C_e represent the initial and equilibrium concentrations (mg g^{-1}), respectively, where V is the volume of the solutions (mL), and m is the amount of the adsorbents (mg).

2.7 Fabrication of FGHs-based supercapacitors with aqueous electrolyte and organic electrolyte

Two slices of FGH (each has a thickness of ~1 mm and a dried-weight of ~1.5 mg) were cut from the as-prepared cylindrical FGHs. For assembly of capacitors with aqueous electrolyte: the slices of FGHs were immersed in 1 M H_2SO_4 aqueous electrolyte overnight to exchange their interior water with electrolyte. Then, the two FGH slices were pressed on two Pt foils separately and separated by a filtrate paper soaked with electrolyte (1 M H_2SO_4). All the components were assembled into a layered structure and sandwiched between two PTFE sheets and immersed in 1 M H_2SO_4 for electrochemical measurements. For assembly of capacitors with organic electrolyte: the HGF slices were first immersed in pure ionic liquid $EMIMBF_4$ under vacuum at 100 ^oC for 12 h to exchange their interior water with $EMIMBF_4$ and then transferred to a $EMIMBF_4$/AN solution with a weight ratio of 1:1 for another 12 h. Subsequently, the HGF slices were pressed on two Pt foils and the supercapacitors were fabricated using the above methods.

2.8 Computational methods

Reduced graphene oxide with 7 benzene rings and one hydroxyl group (G0) was chosen as the pristine RGO in order to simplify the calculations. One R_F-NH_2 chain grafted GO (GF1) and three R_F-NH_2 chains grafted GO (GF3) were used to illustrate the effect of increasing the perfluoroalkyl chains on the changes of electronic structure. For comparison, one alky chain grafted GO (GC1) was also calculated. Their initial structures were shown in Figure S12. The geometries of G0, GC1, GF1 and GF3 were optimized using Becke's three-parameter hybrid functionals combined with the Lee−Yang−Parr correlation functional method (B3LYP)[28, 29] of DFT with the 3-21G* basis set. On the basis of the optimized structures (Figure S11), frontier molecular orbitals have been analyzed at the same level of theory. These calculations were performed using the Gaussian 09 package.

2.9 Materials Characterization

UV-Vis absorption spectra were recorded on a UV-2600 UV-Vis spectrometer (Shimadzu, Japan). FTIR spectra were obtained on a FTIR spectrometer IR Prestige-21 (Shimadzu, Japan). X-ray diffraction (XRD) analyses were carried out on a D-8 ADVANCE X-ray diffractometer (Bruker AXS, Germany). Thermogravimetric analyses (TGA) were conducted on a SDT Q600 (TA, America). X-ray photoelectron spectroscopy (XPS) measurements were taken in a ESCALAB 250 (Thermo Fisher Scientific, America) using a monochromatic Al-Kα X-ray source at 100 W. The scanning electron microscope (SEM) images of the FGH were characterized by QUANTA 200 (FEI, America). The Raman spectra were performed using a LabRAM HR800 Raman spectrometer (HORIBA JY, France). Nitrogen adsorption-desorption isotherms of FGH were measured at 77 K using a Quantachrome Autosorb-6b static volumetric instrument. The cyclic voltammetry (CV) and electrochemical impedance spectroscopy (EIS) measurements were carried out on an electrochemical workstation of a Solartron 1255 frequency response analyzer coupled with Solartron 1287 electrochemical interface. The impedance spectra were recorded by applying a sine

wave with 5 mV amplitude over a frequency range of 100 kHz to 0.01 Hz. The specific capacitances derived from galvanostatic discharge curves were calculated based on the following equation: $C=2(I\Delta t)/(m\Delta V)$, where I is the discharge current, Δt is the time for a full discharge, m is the mass of one electrode, and ΔV represents the potential change after a full discharge.

3. Results and Discussion

The electron withdrawing nature of fluorine made 4-(Perfluorooctyl) aniline (see supporting information) facile reduction of epoxy and carboxyl groups on GO sheets via amide formation (Figure 1a). The covalent bonding of R_F-HN_2 onto GO was evident by a phase transfer of the GO from the water phase into the $CHCl_3$ phase, accompanied by a color change from brown to black (Figure 1b, inset). As expected, the UV-Vis spectrum of GO solution exhibits a maximum at about 227 nm, which can be attributed to π-π* transition of aromatic C-C bond. After refluxing 12 h, the absorption peak shifted to 259 nm, indicating the reduction of GO and the formation of electronic conjugation within the graphene sheets. With the refluxing time increased to 24 h, a slightly blue shift (~ 4 nm) is observed due to the polarization-induced charge effects caused by perfluoroalkyl chains.[30] The FTIR spectrum of GO shows the presence of epoxy (1228 cm^{-1}) and carbonyl (1730 cm^{-1}) groups. The intensities of these IR peaks decrease significantly after chemical attachment of R_F-NH_2 onto GO. In addition, two new peaks at 1153 cm^{-1} and 1200 cm^{-1} (C-F stretching vibration) appear, indicating that perfluorinated alkyl has been chemically grafted onto graphene (Figure 1c).

Importantly, perfluoroalkyl functionalized graphene hydrogel (FGH) can be obtained by heating a good dispersion of GO and R_F-NH_2 without stirring at 100°C for 12 hours (Figure 2a). The resultant FGHs are mechanically strong enough to allow for handling with tweezers (Figure S2). The black FGHs are highly hydrophilic, containing more than 99.7 wt% of water. During hydrothermal treatments, three-dimensional random stacking between flexible graphene sheets most likely

occurred because of the hydrophobic and π-interactions between the graphene nanosheets. It should be noted that hydrogel could not be obtained via the same hydrothermal condition using its alkyl counterpart instead of perfluoroalkyl aniline and GO solution (Figure S3), indicating the critical role of fluorine properties. The structures of the freeze-dried FGHs depend strongly on the mass ratio between graphene oxide and R_F-NH_2. Figure 2b shows the FGHs with different mass ratio of GO and R_F-NH_2, e.g. GO:R_F-NH_2=8:1, 4:1, and 2:1, are prepared and marked as FGH-8, FGH-4, and FGH-2, respectively. The density of freeze-dried FGH-8 is 10.57 mg cm^{-3} and decreases to 8.32 mg cm^{-3} for FGH-2 due to the re-stacking inhibition as R_F-NH_2 increasing. The SEM images of FGH-8 exhibits a well-developed 3D interconnected porous network with macro-pore diameter of about 200 μm (Figure S4). As increasing the content of R_F-NH_2, the macro-pore diameter decreased to 20 μm for FGH-2 (Figure 2c,d). The elemental mapping confirms that perfluoroalkyl chain is uniformly distributed on the graphene foam (Figure 2e-g).

X-ray diffraction (XRD) patterns were used to confirm the interlayer distance of freeze-dried FGHs (Figure 2h). The FGHs exhibit a weak and broad diffraction peak at 24.4°, 24.8°, 25.3° with an interlayer distance of 3.65 Å, 3.58 Å, and 3.51 Å for FGH-8, FGH-4, and FGH-2, respectively, which are much lower than that of GO precursor (7.78 Å) while slightly higher than that of graphite (3.35 Å), indicating the efficient formation of a reduced graphene foam. The decreased interlayer distance is likely because of high degree of reduction as R_F-NH_2 increasing, which is different from the results where the interlayer space of graphene increased when the graphene was functionalized with oxygen or phosphate.[31, 32] Raman spectra also prove the reduction process by monitoring the two signature bands around 1349 cm^{-1} and 1583 cm^{-1}, which are assigned to the D- and G-bands of carbon, respectively (Figure 2i). The I_D/I_G value is calculated to be 0.81 for GO and gradually changes from 1.00 to 1.07 as increasing the content of R_F-NH_2 for the freeze-dried FGHs, confirming that the GO sheets were reduced and their conjugated structures were partly restored.[33, 34] The thermogravimetric analysis (TGA) curves also reveal that the freeze-dried FGHs

are reduced by R_F-NH_2 and become higher thermal stability as the perfluoroalkyl grafted on the surface of GO increased (Figure S5).

The surface chemistry of freeze-dried FGH-2 was further characterized by X-ray photoelectron spectroscopy (XPS). Comparing with GO, the freeze-dried FGH-2 shows two more elements (N, F) (Fig. 2j). The molar ratio of C/O is 2.1 for GO and increases to 4.2 for FGH-2. Furthermore, the value of F/C molar ratio observed is as high as 0.9 and the content of F atom reaches up to 40.7% for FGH-2. The reduction of oxygenous groups is further revealed in C 1s spectra of GO and FGH-2. For GO, four different peaks centered at 284.5, 286.5, 287.1, and 288.6 eV are observed, corresponding to C-C in unoxidized graphite carbon skeleton, C-OH in hydroxyl group, C-O-C in epoxide group, and O-C=O in carboxyl group, respectively. After the reaction with 4-(Perfluorooctyl) aniline, the peaks corresponding to the oxygen-containing groups of FGH-2 are significantly weakened, indicating that a large number of oxygen-containing groups were removed (Figure 2k, Figure S6). Moreover, three new characteristic peaks corresponding to C-N group located at 285.4 eV, C-F_2 located at 291.6 eV and C-F_3 located at 292.5 eV appear, suggesting that 4-(Perfluorooctyl) aniline is grafted onto the GO nanosheets.

Based on the above analysis, we briefly proposed the reduction and functionalization of GO by using 4-(Perfluorooctyl) aniline. The reduction of GO is mainly ascribed to the amine group of 4-(Perfluorooctyl) aniline (Figure S7 in supporting information). (i) The epoxy group can be reduced by the amine groups, where the -NH_2 functionalities may attack the epoxide carbon of GO to convert it into a hydroxyl group accompanying a proton transfer.[35] (ii) In the case of carbonyl and carboxylic groups, the amine groups can react with the carbonyl group via a Michael addition/Schiff base reaction as reported in the literature.[36] The carboxylic groups are very labile, which is easy to be removed from the FGH at high temperature (100℃). (iii) As for the hydroxyl groups, the two adjacent hydroxyl groups may form the transition state of the epoxy group firstly. Then, the resultant epoxy group is reduced by the amine group as demonstrated in (i).[37] After the hydrothermal process, GO was

reduced and functionalized by 4-(Perfluorooctyl) aniline via amide formation synchronously.

The highly porous and mechanically stable freeze-dried FGH provides an ideal platform for high-efficiency adsorption that is crucial for extraction of specific substances, such as organic pollutants. As shown in the Figure 3a, freeze-dried FGH-2 was put into the mixture of n-Hexane and RhB/H_2O solution. After two hours, the rhodamine B (RhB) in water becomes colorless. Figure 3b reveals that the characteristic peak of RhB with the concentration of 2 mg mL^{-1} becomes too weak to be observed by UV-Vis spectrum after 10 min absorption, suggesting the high efficiency for rapid removal of RhB.

Methylene blue (MB) as a typical representative dye extensively exists in wastewater from industry and it is not susceptible to degradation through some conventional methods, so it is easy to cause serious environmental pollution problems. Here, MB was selected as a mode organic dye to study the capability of dye adsorption by the freeze-dried FGH-2 sample. In a typical procedure, a certain amount of sample was added to the 100 ml MB (10 mg mL^{-1}) at room temperature. Then, UV-Vis spectra of the solution were measured at different time to calculate the adsorption efficiency. The characteristic peak of MB becomes very weak after 30 h adsorption, suggesting the high efficiency for rapid removal of MB (Figure S8). The adsorption isotherm fits the Langmuir model which gives a maximum adsorption capacity (Q_m) of 227 mg g^{-1} (Figure 3c), much higher than that of titanium dioxide functionalized graphene foam,[38] indicting the sample hold great application potential as high efficient adsorbents in environment cleaning field.

Inspired by our previous studies on RGO for energy storage,[39] the FGHs were cut into self-supported slices with a thickness of ≈1 mm and a dried-weight of ≈1.5 mg, which were further pressed on two platinum foils and used directly as supercapacitor electrodes in 1 M H_2SO_4 aqueous electrolyte. It was found that the cyclic voltammetric (CV) profile of FGH-4 and FGH-2 retain a relatively similar rectangular shape without obvious distortion compared to that of FGH-8 at scan rates from 5 to 100 mV s^{-1} within a potential window of 0.8 V (Figure 4a, Figure S9).

Galvanostatic charge-discharge (GCD) tests reveal linear and symmetric curves, suggesting good capacitive characteristic of FGH supercapacitor. With the increase in the fluoroalkyl chain contents, the CV curves become more rectangular. FGH-2 device reveals the most rectangular shape than FGH-8, FGH-4 and pristine graphene hydrogel (GH) devices at high scan rate of 200 mV s^{-1} (Figure S10). Correspondingly, the GCD curves also show that the discharge time becomes longer as the fluoroalkyl chain content increases for all the FGH devices, indicating that the capacitive behaviour of the device could be greatly improved by increasing the fluoroalkyl chains content (Figure S10).

For a deep understanding of FGH structures, a Nyquist plot of the FGH-8, FGH-4, and FGH-2 devices was conducted in a frequency range 0.01 Hz to 100 kHz at open-circuit voltage with an ac amplitude of 5 mV as shown in Figure 4c. For all FGHs device, the straight lines are nearly parallel to the imaginary axis, revealing an ideal capacitive behaviour of the devices. The series resistances of the devices were measured to be about 6.3 Ω for FGH-8, 5.4 Ω for FGH-4 and 4.2 Ω for FGH-2. It can be seen that at high frequencies the FGH-2 electrode displays the smallest semicircle, which is related to the lowest charge transfer resistance, and a transition to linearity at low frequency which exhibits an ideal capacitive behavior.[40] Additionally, the FGH-2 device shows much shorter Warburg region portion compared with FGH-8 and FGH-4, which indicated better ion diffusion efficiency due to smaller contact resistance among the material and ion.[41] The dependence of the phase angle on the frequency reveals that the relaxation time constant τ_0 is about 6.29 s ($\tau_0 = 1/f_0$) for FGH-8 and decreased to 2.51 s for FGH-2 device. This increased frequency response of the FGHs can be accounted for by the large and accessible surface area of the graphene foam, whose exposed graphene sheets enhance the ion transport rate in the device.[42]

The specific capacitances of these electrodes in the two-electrode system were calculated based on the mass of FGHs. At the current density of 1.0 A g^{-1}, the highest gravimetric capacitance of the FGH-2 electrode is 321.6 F g^{-1}, while the capacitance of FGH-8, FGH-4 is 279.1 F g^{-1} and 292.9 F g^{-1} respectively. The gravimetric

capacitance of the FGH-2 electrode (321.6 F g^{-1}) is higher than that of porous graphene and[43-45] comparable to that of heteroatoms doped graphene,[46] and are among the highest values achieved in chemically modified graphene electrode materials.[22, 47] Furthermore, with increasing the current density up to 42 A g^{-1}, the specific capacitances of FGH-2 first decrease and then remain stable at about 281.2 F g^{-1} (above 87% of the initial value at 1.0 A g^{-1}), highlighting the excellent rate capability of FGH-2 (Figure 4e). Good cycling stability is another important characteristic for high-performance supercapacitors. Figure 4f reveals the cycle performance of the FGH-2 samples measured at current density of 20.8 A g^{-1} for 10,000 cycles. Afterward, the capacitance was 94.2% of the initial capacitance, indicating excellent long-term stability of the FGH-2 electrode.

The electrical conductivity of the compressed hydrogel films were also measured by four-point probe, which was about 340, 420, 560 S m^{-1} for FGH-8, FGH-4, and FGH-2 electrode film, respectively. In our work, R_F-NH_2 was used as reducing agent and functionalizing molecule synchronously. Although the fluoroalkyl chains are not electrically conductive, the conductivity of the electrode films increased as the content of R_F-NH_2 increased. This is because that the degree of reduction was increased. In addition, much amount of R_F-NH_2 grafted on graphene sheets will reduce the π-π stacking, leading to a large accessible surface area for electrolyte ions. The high conductivity and large surface area of FGH-2 account for its enhanced capacitive behavior.

We also examined an organic electrolyte, which would allow the operation of the devices at higher voltages, thus achieving higher energy densities. In this case, a similar two-electrode device was constructed using FGH-2 as the electrode material and 1-ethyl-3-methylimidazolium tetrafluoroborate/acetonitrile ($EMIMBF_4$/AN) as the electrolyte and the performance is shown in Figure 5. As expected, The CV curves are rectangular in shape from 0 to 3.5 V at a scan rate from 50 mV s^{-1} to 1000 mV s^{-1}. The galvanostatic charge-discharge plots with negligible IR drops (<0.01v) are symmetrical triangles. Both of them indicate a near-ideal capacitive behavior of FGH-2 device with good rate performance. A resistance of 6.8 Ω obtained by

extrapolating the vertical portion of the plot to the real axis confirmed a low series resistance value of the device (Figure S11). The measured gravimetric capacitance is 303.8 F g^{-1} at 3.5 V and a current density of 2.1 A g^{-1}. A very high energy density of 129.3 W h kg^{-1} was achieved with a reasonably high power density of 182.3 kW kg^{-1} for FGH-2 device in the $EMIMBF_4$/AN system.

To explain the electrochemical results, it is important to consider the hierarchical structured network that exerts such a significant influence on charge storage. This consideration is closely related to the surface area. Given that the fluoroalkyl functionalized hydrogels are directly used as electrodes by ions exchange without freeze-drying, the specific surface areas were determined by methylene blue dye adsorption method. With this approach the solvated surface area is 1182 m^2 g^{-1} for FGH-8, 1249 m^2 g^{-1} for FGH-4 and 1325 m^2 g^{-1} for FGH-2, respectively (Table S1), which is about half of theoretical surface area of single-layer graphene ($\approx$2630 m^2 g^{-1}) and similar to the surface area of graphene hydrogel functionalized by hydroquinones (1380 m^2 g^{-1})[22]. The increased surface area with increasing the fluoroalkyl chains accounts for the increased specific capacitance to some extent. In addition, the pore size of the freeze-dried FGHs determined by nitrogen adsorption-desorption measurements was in the range of 3-60 nm (Figure S12), which can facilitate ions diffusion into the pores as well as electron transport throughout the entire graphene foam.[48]

Furthermore, since the capacitance is related to the electronic structures of graphene,[49, 50] which can be altered from chemical modification, the changes of electronic structure of the perfluoroalkyl functionalized graphene were simulated by the density functional theory (DFT) (Figure 6). Reduced graphene oxide with 7 benzene rings and one hydroxyl group (G0) was chosen as the pristine RGO in order to simplify the calculations. One R_F-NH_2 chain grafted GO (GF1) and three R_F-NH_2 chains grafted GO (GF3) were used to illustrate the effect of increasing the perfluoroalkyl chains on the changes of electronic structure. For comparison, one alky chain grafted GO (GC1) was also calculated. Their initial structures and corresponding the contours of the highest occupied molecular orbital (HOMO) are

shown in Figure S11. After introduction of perfluoroalkyl chains, GF1 lowers the lowest unoccupied molecular orbital (LUMO) energy levels and increases HOMO energy levels, leading to a low band gap of 1.33 eV, lower than that of GC1 (Figure 6). Further increasing the perfluoroalkyl chain leads to a more decreased bad gap to 1.29 eV for GF3, due to the strong electron withdrawing nature of fluorine. It is noteworthy that GF3 show the distinctly denser distribution of the first five frontier occupied molecular orbitals energy levels and better electron delocalizability than those of others (Figure 6 and Figure S13), which is crucial for efficient charge transport.[51, 52] Such results suggest that the possibility of tuning the electronic properties of perfluoroalkyl functionalized graphene is partially attributed to the strong electron withdrawing nature of fluorine.

4. Conclusions

In summary, we have developed a simple and general solution-based process to introduce perfluoroalkyl chains onto GO by amidation. The as-prepared FGHs exhibit outstanding absorption ability and electrochemical performances including ultrahigh specific capacitances and excellent cycling stability in the aqueous electrolyte and organic electrolyte. It should be noted that although perfluorinated moieties are non-conductive, the decreased interface resistance and increased surface area combined with the better electron delocalizability of the perfluoroalkyl functionalized graphene as the contents of perfluoroalkyl chains increasing indicate that perfluoroalkyl functionalized graphene is adequate for employment as a conducting electrode without significant hindrance of electron transport. Our work clearly reveals that the properties of graphene can be greatly promoted by elaborated combination of surface functionalization and hierarchical structures of graphene sheets.

Acknowledgements

We acknowledge the support by Program for Scientific Research Innovation Team in College and Universities of Shandong Province, the National Natural Science Foundation of China (21204044), the Natural Science Foundation of Shandong

Province for Excellent Young Scholars (ZR2015JL009), Project of Natural Science Foundation of Shandong Province (ZR2014EMM020), Shandong Outstanding Young Scientist Award Fund (BS2012CL028) and Ji'nan Overseas Students Pioneer Plan (20120202).

References

1. K. S. Novoselov, A. K. Geim, S. V. Morozov, D. Jiang, Y. Zhang, S. V. Dubonos, I. V. Grigorieva and A. A. Firsov, *Science*, 2004, **306**, 666-669.
2. A. K. Geim, *Science*, 2009, **324**, 1530-1534.
3. L.-H. Liu, M. M. Lerner and M. Yan, *Nano Lett.*, 2010, **10**, 3754-3756.
4. G. Eda and M. Chhowalla, *Adv. Mater.*, 2010, **22**, 2392-2415.
5. D. K. Samarakoon and X.-Q. Wang, *ACS nano*, 2009, **3**, 4017-4022.
6. M. Pumera and C. H. A. Wong, *Chem. Soc. Rev.*, 2013, **42**, 5987-5995.
7. F. Karlický, K. Kumara Ramanatha Datta, M. Otyepka and R. Zbořil, *ACS nano*, 2013, **7**, 6434-6464.
8. J. T. Robinson, J. S. Burgess, C. E. Junkermeier, S. C. Badescu, T. L. Reinecke, F. K. Perkins, M. K. Zalalutdniov, J. W. Baldwin, J. C. Culbertson, P. E. Sheehan and E. S. Snow, *Nano Lett.*, 2010, **10**, 3001-3005.
9. O. Leenaerts, H. Peelaers, A. D. Hernández-Nieves, B. Partoens and F. M. Peeters, *Phys. Rev. B.*, 2010, **82**, 195436.
10. S. Eigler and A. Hirsch, *Angew. Chem. Int. Ed.*, 2014, **53**, 7720-7738.
11. D. R. Dreyer, S. Park, C. W. Bielawski and R. S. Ruoff, *Chem. Soc. Rev.,* 2010, **39**, 228-240.
12. S. Niyogi, E. Bekyarova, M. E. Itkis, J. L. McWilliams, M. A. Hamon and R. C. Haddon, *J. Am. Chem. Soc.*, 2006, **128**, 7720-7721.
13. E. Bekyarova, M. E. Itkis, P. Ramesh, C. Berger, M. Sprinkle, W. A. de Heer and R. C. Haddon, *J. Am. Chem. Soc.*, 2009, **131**, 1336-1337.
14. Y. Xu, Z. Liu, X. Zhang, Y. Wang, J. Tian, Y. Huang, Y. Ma, X. Zhang and Y. Chen, *Adv. Mater.*, 2009, **21**, 1275-1279.
15. N. Liu, F. Luo, H. Wu, Y. Liu, C. Zhang and J. Chen, *Adv. Funct. Mater.*, 2008, **18**, 1518-1525.
16. S. Song, Y. Xue, L. Feng, H. Elbatal, P. Wang, C. N. Moorefield, G. R. Newkome and L. Dai, *Angew. Chem. Int. Ed.*, 2014, **53**, 1415-1419.
17. H.-G. Jung, C. S. Yoon, J. Prakash and Y.-K. Sun, *J. Phys. Chem. C*, 2009, **113**, 21258-21263.

18. R. R. Nair, W. C. Ren, R. Jalil, I. Riaz, V. G. Kravets, L. Britnell, P. Blake, F. Schedin, A. S. Mayorov, S. J. Yuan, M. I. Katsnelson, H. M. Cheng, W. Strupinski, L. G. Bulusheva, A. V. Okotrub, I. V. Grigorieva, A. N. Grigorenko, K. S. Novoselov and A. K. Geim, *Small*, 2010, **6**, 2877-2884.
19. K. J. Jeon, Z. Lee, E. Pollak, L. Moreschini, A. Bostwick, C. M. Park, R. Mendelsberg, V. Radmilovic, R. Kostecki, T. J. Richardson and E. Rotenberg, *ACS Nano,* 2011, **5**, 1042-1046.
20. Y. Xu, K. Sheng, C. Li and G. Shi, *ACS nano*, 2010, **4**, 4324-4330.
21. X. M. Feng, N. Chen, Y. Zhang, Z. Z. Yan, X. F. Liu, Y. W. Ma, Q. M. Shen, L. H. Wang and W. Huang, *J. Mater. Chem. A*, 2014, **2**, 9178-9184.
22. Y. Xu, Z. Lin, X. Huang, Y. Wang, Y. Huang and X. Duan, *Adv. Mater.*, 2013, **25**, 5779-5784.
23. X. M. Feng, Z. Z. Yan, N. N. Chen, Y. Zhang, Y. W. Ma, X. F. Liu, Q. L. Fan, L. H. Wang and W. Huang, *J. Mater. Chem. A*, 2013, **1**, 12818-12825.
24. Y. Xu, Q. Wu, Y. Sun, H. Bai and G. Shi, *ACS nano*, 2010, **4**, 7358-7362.
25. G. Zhu, Z. He, J. Chen, J. Zhao, X. Feng, Y. Ma, Q. Fan, L. Wang and W. Huang, *Nanoscale*, 2014, **6**, 1079-1085.
26. X. Feng, Z. Yan, N. Chen, Y. Zhang, X. Liu, Y. Ma, X. Yang and W. Hou, *New J. Chem.*, 2013, **37**, 2203-2209.
27. M. J. McAllister, J.-L. Li, D. H. Adamson, H. C. Schniepp, A. A. Abdala, J. Liu, M. Herrera-Alonso, D. L. Milius, R. Car, R. K. Prud'homme and I. A. Aksay, *Chem. Mater.*, 2007, **19**, 4396-4404.
28. A. D. Becke, *J. Chem. Phys.*, 1993, **98**, 5648-5652.
29. Y.-q. Ding, Y.-z. Cui and T.-d. Li, *J. Phys. Chem. A*, 2015, **119**, 4252-4260.
30. Y. Wang, W. C. Lee, K. K. Manga, P. K. Ang, J. Lu, Y. P. Liu, C. T. Lim and K. P. Loh, *Adv. Mater.*, 2012, **24**, 4285-4290.
31. J. B. Goods, S. A. Sydlik, J. J. Walish and T. M. Swager, *Adv. Mater.*, 2014, **26**, 718-723.
32. Z. Bo, X. Shuai, S. Mao, H. Yang, J. Qian, J. Chen, J. Yan and K. Cen, *Sci. Rep.*, 2014, **4**, 4684.
33. K. N. Kudin, B. Ozbas, H. C. Schniepp, R. K. Prud'homme, I. A. Aksay and R. Car, *Nano lett.*, 2008, **8**, 36-41.
34. J. Liu, L. Liu, X. Wu, X. Zhang and T. Li, *New. J. Chem.*, 2015, **39**, 5272-5281.
35. N. H. Kim, T. Kuila and J. H. Lee, *J. Mater. Chem. A*, 2013, **1**, 1349-1358.
36. L. Q. Xu, W. J. Yang, K.-G. Neoh, E.-T. Kang and G. D. Fu, *Macromolecules*, 2010, **43**, 8336-8339.
37. H. Liu, T. Kuila, N. H. Kim, B.-C. Ku and J. H. Lee, *J. Mater. Chem. A*, 2013, **1**, 3739-3746.

38. Z. Zhang, F. Xiao, Y. Guo, S. Wang and Y. Liu, *ACS Appl. Mater. Inter.*, 2013, **5**, 2227-2233.
39. L. Liu, Y. Yu, C. Yan, K. Li and Z. Zheng, *Nat. Commun.*, 2015, **6**, 7260.
40. M. D. Stoller, S. Park, Y. Zhu, J. An and R. S. Ruoff, *Nano lett.*, 2008, **8**, 3498-3502.
41. L. L. Zhang and X. S. Zhao, *Chem. Soc. Rev.*, 2009, **38**, 2520-2531.
42. Y. Shim, Y. Jung and H. J. Kim, *J. Phys. Chem. C*, 2011, **115**, 23574-23583.
43. M. F. El-Kady, V. Strong, S. Dubin and R. B. Kaner, *Science*, 2012, **335**, 1326-1330.
44. X. Yang, J. Zhu, L. Qiu and D. Li, *Adv. Mater.*, 2011, **23**, 2833-2838.
45. Y. Xu, Z. Lin, X. Zhong, X. Huang, N. O. Weiss, Y. Huang and X. Duan, *Nat. Commun.*, 2014, **5**, 4554.
46. H. M. Jeong, J. W. Lee, W. H. Shin, Y. J. Choi, H. J. Shin, J. K. Kang and J. W. Choi, *Nano lett.*, 2011, **11**, 2472-2477.
47. Y. Fang, B. Luo, Y. Jia, X. Li, B. Wang, Q. Song, F. Kang and L. Zhi, *Adv. Mater.*, 2012, **24**, 6348-6355.
48. P. Simon and Y. Gogotsi, *Nat. Mater.*, 2008, **7**, 845-854.
49. M. Bagge-Hansen, B. C. Wood, T. Ogitsu, T. M. Willey, I. C. Tran, A. Wittstock, M. M. Biener, M. D. Merrill, M. A. Worsley, M. Otani, C.-H. Chuang, D. Prendergast, J. Guo, T. F. Baumann, T. van Buuren, J. Biener and J. R. I. Lee, *Adv. Mater.*, 2015, **27**, 1512-1518.
50. H. Ji, X. Zhao, Z. Qiao, J. Jung, Y. Zhu, Y. Lu, L. L. Zhang, A. H. MacDonald and R. S. Ruoff, *Nat. Commun.*, 2014, **5**, 3317.
51. G. M. Yang, H. Z. Zhang, X. F. Fan and W. T. Zheng, *J. Phys. Chem. C*, 2015, **119**, 6464-6470.
52. S. M. Mousavi-Khoshdel and E. Targholi, *Carbon*, 2015, **89**, 148-160.

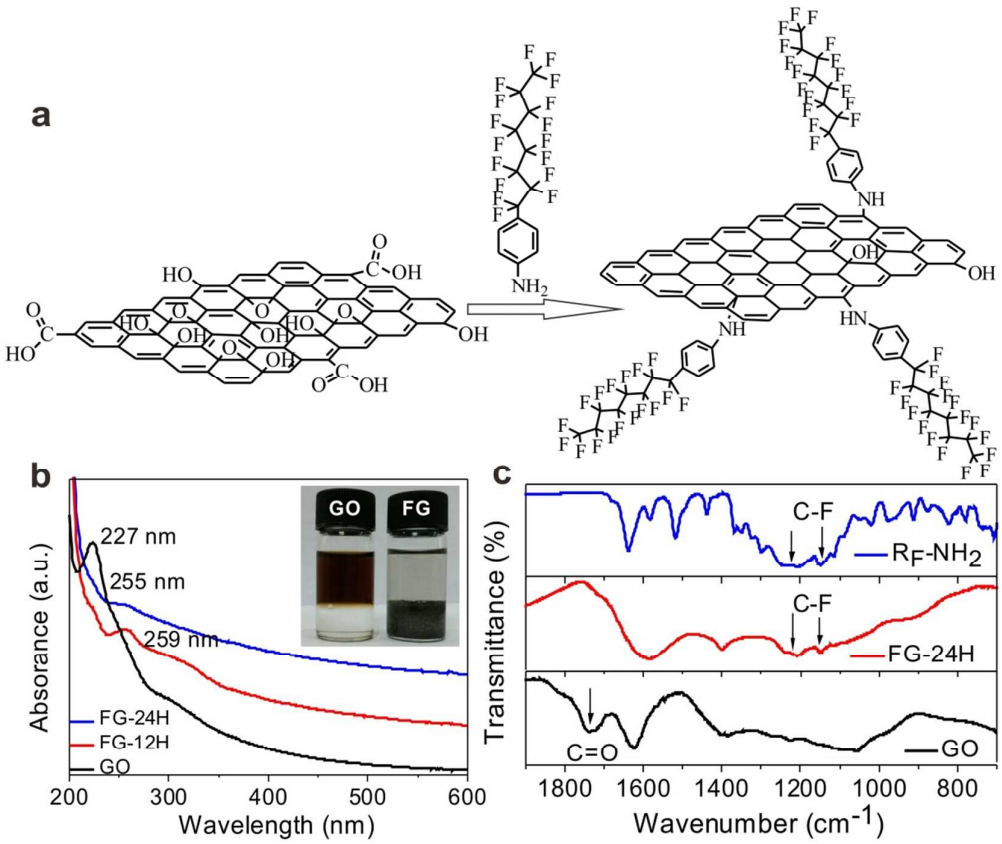

Figure 1. (a) Schematic of the reaction of GO with R_F-NH_2; UV-Vis (b) and FTIR (c) spectra of GO aqueous dispersions and functionalized graphene (FG) with refluxing time of 12 h and 24 h; a dispersion of GO precursors and FG in $H_2O/CHCl_3$ mixtures were inserted in (b).

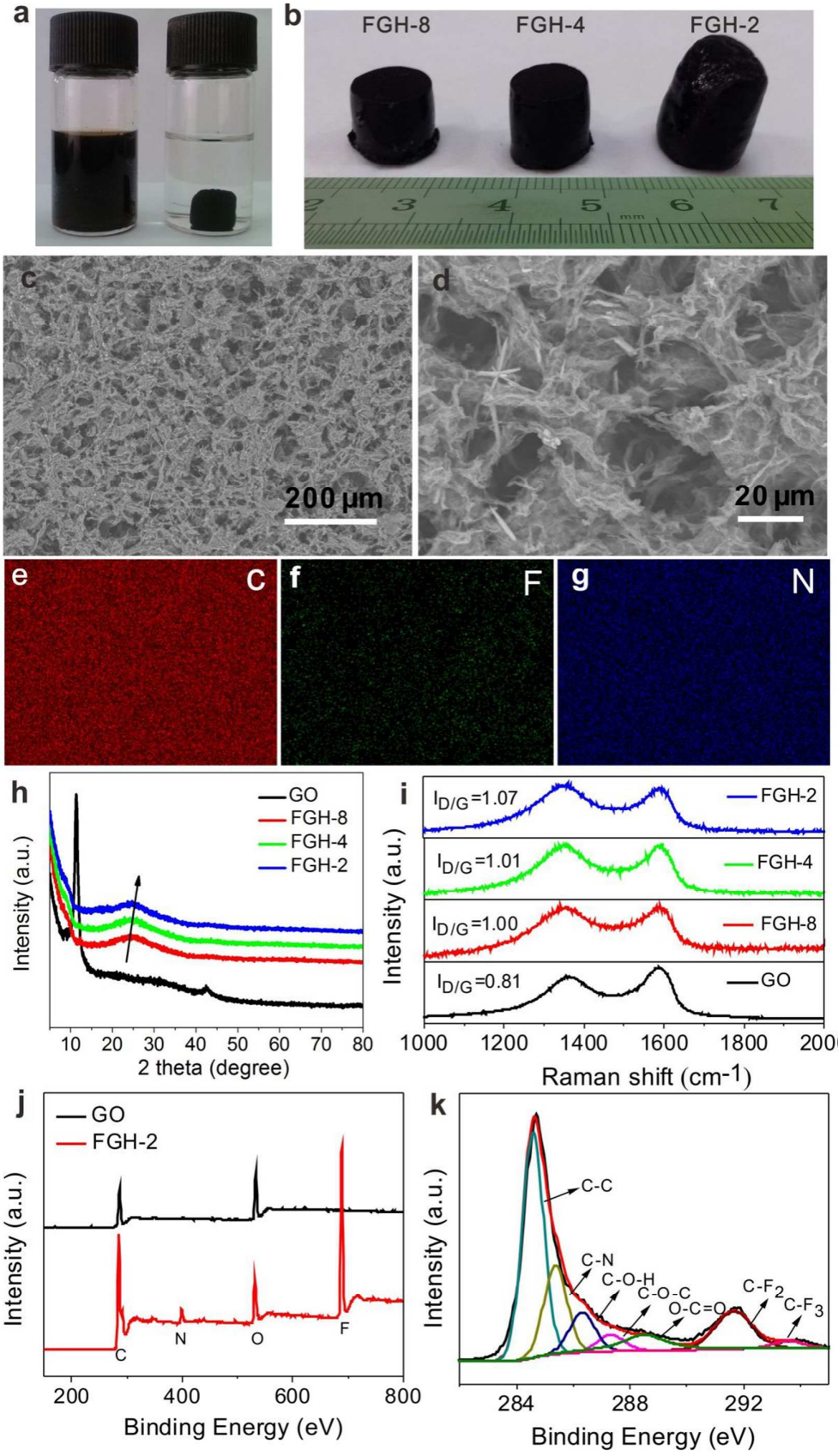

Figure 2. (a) Photographs of an aqueous dispersion of GO and the as-prepared FGH; (b) Photographs of different content of fluoroalkyl chains of freeze-dried FGHs; (c,d) low and high magnification SEM images of FGH-2; (e,f,g) elemental mapping of FGH-2 in Figure d for C,F,N, respectively; XRD spectra (h) and Raman patterns (i) of GO and different FGHs; (j) XPS spectra of GO and FGH-2; (k) XPS spectra of C 1s profile for freeze-dried FGH-2.

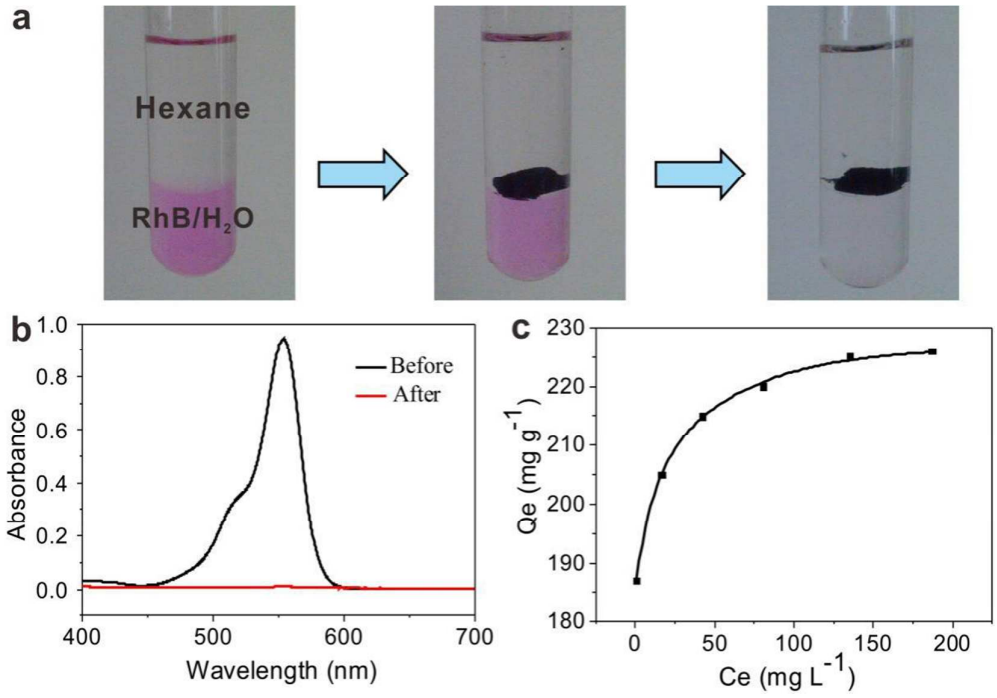

Figure 3. (a) Photographs of FGH-2 in n-Hexane and RhB/H_2O solution; (b) UV-Vis absorption spectra of the RhB before and after FGH-2 absorption; (c) Adsorption isotherms of MB on FGH-2, Qe (mg g^{-1}) is the amount of dyes absorbed at equilibrium, Ce (mg L^{-1}) is the equilibrium solute concentration.

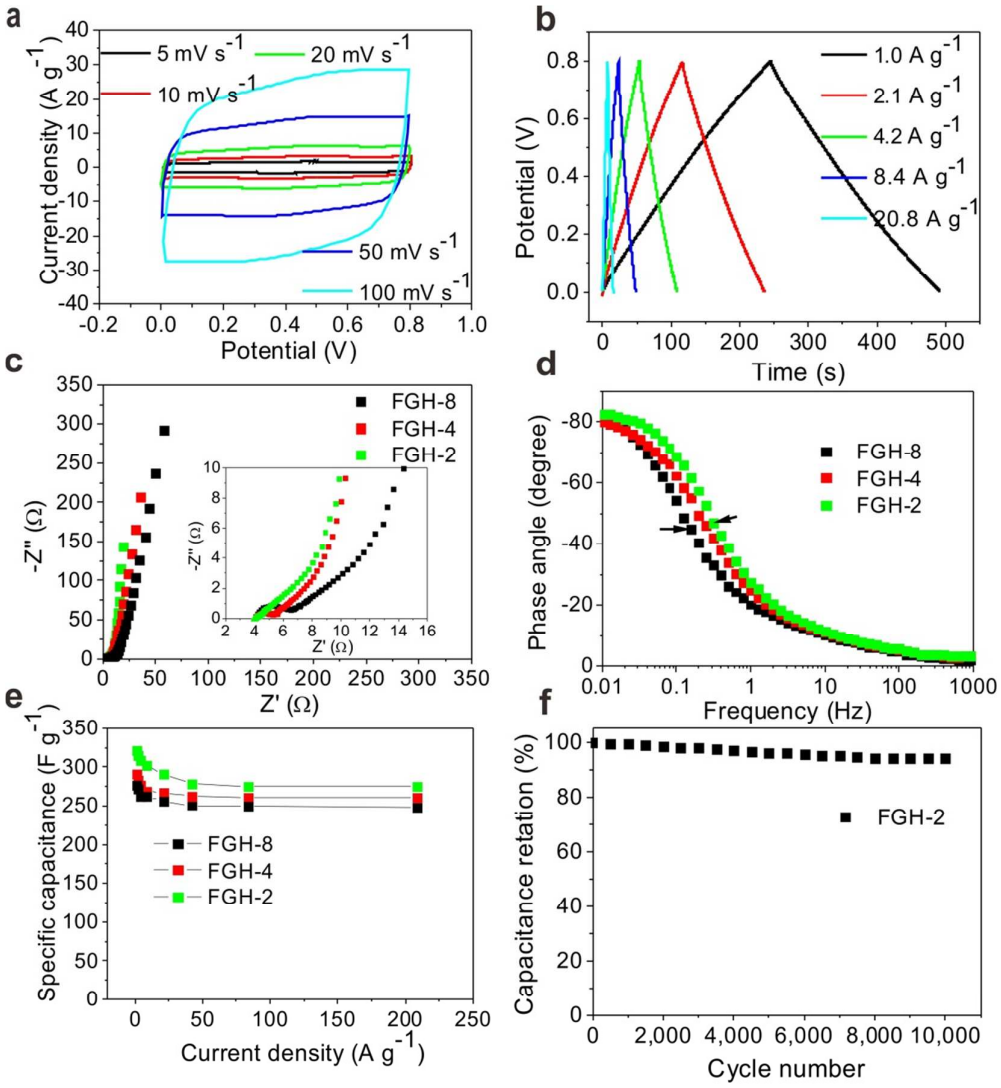

Figure 4. (a) CV curves of the FGH-2 device at scan rates from 5 to 100 mV s^{-1}; (b) GCD curves of the FGH-2 device at different current densities; (c) Electrochemical impedance plots and inset shows an enlarged scale; (d) Bode plots of phase angle versus frequency; (e) Gravimetric specific capacitances of the FGH electrodes; (f) Cycling stability of FGH-2 device.

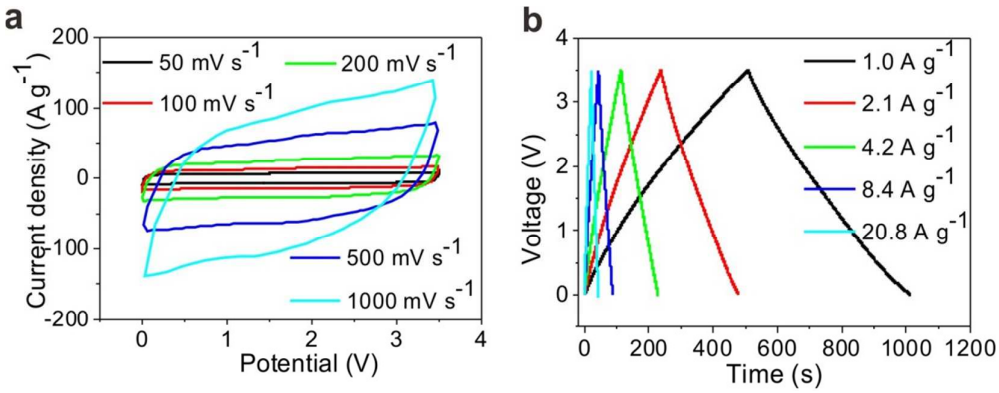

Figure 5. Performances of FGH-2 in $EMIMBF_4$/AN electrolytes. (a) CV curves of FGH-2 device at scan rates from 50 to 1000 mv s^{-1}; (b) GCD curves of the device at different current densities.

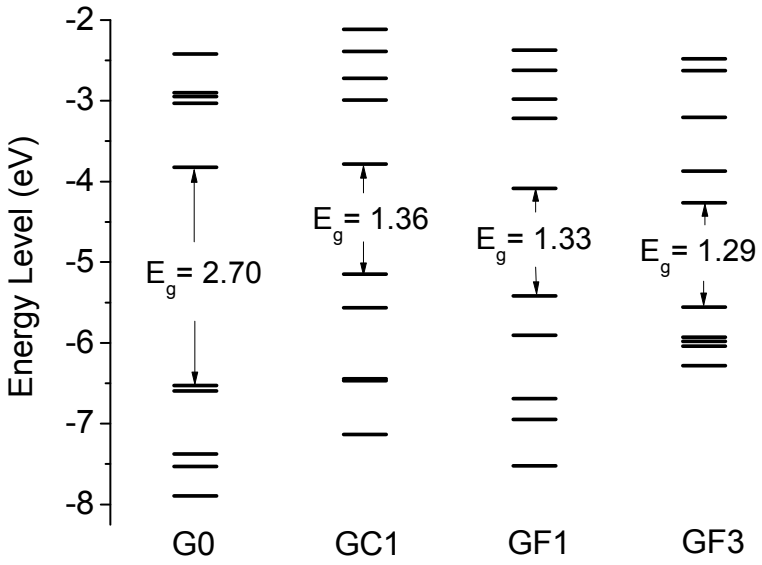

Figure 6. Calculated electron-energy levels for frontier molecular orbitals of G0, GC1, GF1 and GF3 using the DFT method at the B3LYP/3-21G* level.

The table of contents

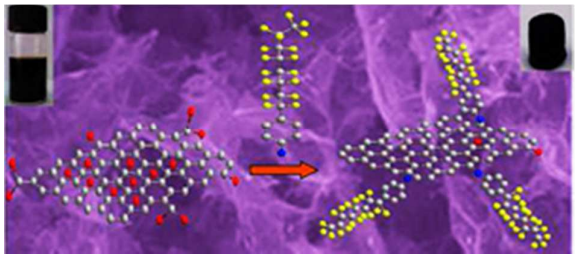

Perfluoroalkyl functionalized graphene hydrogels could be achieved by a hydrothermal method, which exhibit outstanding absorption ability and electrochemical performances.